



Characterization and photoelectrochemical performance of Zn-doped TiO₂ films by sol–gel method

Li-ying QIAO^{1,2}, Feng-yu XIE³, Ming-hui XIE¹, Cai-hua GONG¹, Wei-lang WANG¹, Jia-cheng GAO¹

1. College of Materials Science and Engineering, Chongqing University, Chongqing 400045, China;
2. National Engineering Research Center for Magnesium Alloys, Chongqing University, Chongqing 400044, China;
3. College of Chemistry and Materials Science, Sichuan Normal University, Chengdu 610068, China

Received 16 March 2015; accepted 4 December 2015

Abstract: Zn-doped TiO₂ (Zn–TiO₂) thin films were prepared by the sol–gel method on titanium substrates with heat treatment at different temperatures. The effects of heat treatment temperatures and Zn doping on the structure, photocathodic protection and photoelectrochemical properties of TiO₂ thin films were investigated. It is indicated that the photoelectrical performance of the Zn–TiO₂ films is enhanced with the addition of Zn element compared with the pure-TiO₂ film and the largest decline by 897 mV in the electrode potential is achieved under 300 °C heat treatment. SEM–EDS analyses show that Zn element is unevenly distributed in Zn–TiO₂ films; XRD patterns reveal that the grain size of Zn–TiO₂ is smaller than that of pure-TiO₂; FTIR results indicate that Zn–O bond forms on Zn–TiO₂ surface. Ultraviolet visible absorption spectra prove that Zn–TiO₂ shifts to visible light region. Mott–Shottky curves show that the flat-band potential of Zn–TiO₂ is more negative and charge carrier density is bigger than that of pure-TiO₂, implying that under the synergy of the width of the space-charge layer, carrier density and flat-band potential, Zn–TiO₂ with 300 °C heat treatment displays the best photocathodic protection performance.

Key words: TiO₂ films; Zn-doping; photocathodic protection; photoelectrochemical activity; sol–gel method

1 Introduction

TiO₂ semiconductor materials have attracted much attention for their non-toxic nature, efficiency, and stable photovoltaic activity, thus having great advantages and broad application prospects in the field of photovoltaic conversion, catalytic oxidation of environmental pollutants and sensors [1–3]. So far, TiO₂ films have been used as a surface protective layer of a variety of metals [4–6] for being stable, easily recyclable and insoluble in common acid and alkaline solution; and moreover, intensive attention has been focused on the researches of TiO₂ films for photocathodic protection of metals recently [7–10].

In this technique, photo-generated electron-hole pairs are created in the conduction band of TiO₂ under the ultraviolet illumination. These electrons can transfer to the metal in connect with TiO₂ films and making the electrode potential of the metal more negative than its

corrosion potential and the metal corrosion is controlled. Unlike sacrificial anodes in cathodic protection system, TiO₂ films theoretically can act as a non-sacrificial photoanode and provide long-term cathodic protection for metals, because the anodic reaction is not the decomposition of TiO₂ itself but the oxidation of water and/or adsorbed organic species by the photogenerated holes [11]. However, nano-TiO₂ cathodic protection has been limited in its practical applications due to its large band gap, small absorption field of solar energy and the fast recombination of electron-hole pair. Those problems cause the pure TiO₂ films cannot decrease the electrode potential of the metal substrate enough. Furthermore, as the photoanode, TiO₂'s conduction band potential should be lower than the corrosion potential of the metal which is to be protected, to make sure photo-generated electrons from the conduction band transfer to the protected metal.

Therefore, how to improve the photocathodic protection properties of TiO₂ has become the current

research hotspot. The surface modification with low band gap semiconductors (CdS [9], CdSe [12], etc) and metal (Fe [10], Ni [13], Ce [7], etc) or nonmetal (N [14]) element ion doping technique have been used to improve the photocathodic protection performance. Metal ion doping can introduce defects in the semiconductor lattice or change the degree of crystallinity, thus affecting the electron-hole recombination. Currently, researches on Zn element ion doping of nano-TiO₂ have been reported, but most of the work focused on the study of the photoelectric conversion efficiency and photocatalytic activity of TiO₂ to further improve its performance in photocatalysis and solar cells, etc. There is little research on the application of cathodic protection of metal. ZHANG et al [15] believed that a trace amount of Zn²⁺ into the TiO₂ promoted the separation of photo-generated charges and depressed the recombination because of the decreasing of surface trap states and the strong interface built in electric field. LI et al [16] reported that codoping V and Zn led to formation of multi-dopant energy level within the band gap of TiO₂, and these impurities serve as trapping centers to retard charge recombination. WANG and TENG [17] thought that owing to lower density of empty trap states, Zn-doped TiO₂ possessed efficient electron transport in dye-sensitized solar cells.

In this work, Zn-doped TiO₂ (Zn-TiO₂) thin films were prepared by the sol-gel method on titanium substrates instead of the conventional ITO glass substrate. This not only avoids the introduction of impurities, but also the shortcoming that ITO cannot withstand high-temperature heat treatment. The potential of the Ti substrate dropped by 897 mV, which is higher than the potential drop of ITO (most of the reported results are 200–700 mV). The impacts of Zn-doping at different heat-treatment temperatures on the physical properties and photo-cathode protective effect of TiO₂ thin films were discussed, including the flat-band potential, Fermi level, the charge carrier density (N_d) and the space-charge layer width (W). It will provide theoretical and technical guidance for the photocathodic protection technology.

2 Experimental

2.1 Preparation of films

The Zn-TiO₂ sol was prepared by a sol-gel process with the following procedure: a certain amount of ZnCl₂ was dissolved in distilled water, and analytically pure TiCl₄ was added slowly, the solution then was heated to 95 °C on a magnetic stirrer, until it turned to light blue; after the solution was cooled, NH₄OH was dropped into it, then TiO₂ deposition was obtained and washed with distilled water to remove Cl⁻; after ultrasonic dispersion

Zn-TiO₂ sol was attained. And the mole ratio of Zn to Ti was 1%. Besides, the pure TiO₂ sol was also prepared for a comparison.

Pure titanium sheets (20 mm × 20 mm × 2 mm) were used as the metal substrate. Before coating, the surface of the metal was polished with SiC paper up to 1000 grit, then degreased in 500 mL solution of 10 g NaOH and 20 mL H₂O₂ for 1 h, then immersed in solution of $n(\text{HCl}):n(\text{H}_2\text{O})=1:5$ for 30 min, finally, after washing with distilled water and dried naturally. The titanium sheets were put in a spin coater, Zn-TiO₂/TiO₂ sol was dropped to titanium surface, until the sol spread across the surface at a certain rotation speed to get wet Zn-TiO₂/TiO₂ films, then the sample was dried in the oven at 80 °C for 10 min; and three-layered Zn-TiO₂/TiO₂ films were obtained by repeating the deposition and drying procedures. The samples subsequently were heat-treated in a furnace for 2 h at 100, 300, and 500 °C respectively.

2.2 Characterization

The crystalline structures of the TiO₂/Zn-TiO₂ gels were identified by X-ray diffraction (XRD, D/max-1200) using Cu K_α radiation at 40 kV and 200 mA. The morphology and composition of the Zn-TiO₂ films were analyzed by field emission scanning electron microscopy (SEM, Amray-X 2000, 15 kV) and energy dispersion spectroscopy (EDS, XL30-TMP, 20 kV). The groups of Zn-TiO₂ films were examined by FTIR (Nicolet 5DXC) in the test wavelength range of 400–4000 cm⁻¹. Ultra-violet visible (UV-vis) absorption spectra were recorded by a diffuse reflectance UV-vis spectrometer (UV2100) at a scanning speed of 5 nm/s.

The electrochemical experiments were carried out by a three-electrode cell (CHI660D) in 0.2 mol/L Na₂SO₄ solution, using the TiO₂/Zn-TiO₂ films with an exposed area of 1 cm² as a working electrode, platinum as a counter electrode and saturated calomel electrode (SCE) as a reference electrode, 150 W mercury lamp as the source of illumination. Open-circuit potential (OCP)-time curves in the presence and absence of light illumination were tested. Mott-Shottky plots were measured under illuminated condition to analyze the semiconductor performance of the TiO₂ films at frequency of 1000 Hz with AC excitation signal voltage of 10 mV.

3 Results and discussion

3.1 XRD analysis

Figure 1 shows XRD patterns of Zn-TiO₂ and pure-TiO₂ gels. As shown in Fig. 1, after heat-treatment, the highest diffraction peaks of the Zn-TiO₂ and pure-TiO₂ stand at 25.3° and 25.4° respectively, as a

characteristic diffraction peak of anatase (A(101)), indicating that the gels are mainly composed of anatase-TiO₂; after the heat treatment of 300 °C, the peak of brookite (B(121)) appears. After the heat treatment of 100 °C, XRD diffraction peak is weak and wide, indicating that the degree of crystallinity is low. As the temperature increases, the peaks become sharp and strong, indicating that the anatase content increases, and also the grain size becomes larger.

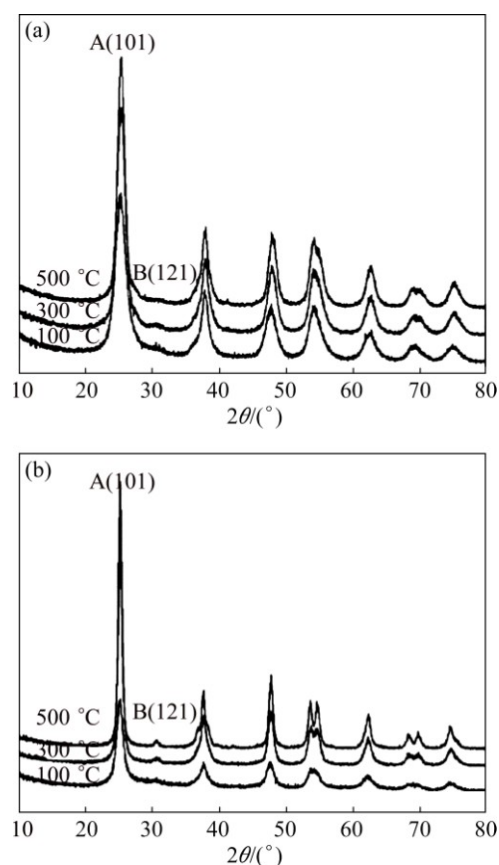


Fig. 1 XRD patterns of Zn-TiO₂ (a) and pure-TiO₂ (b) gels after various heat treatments

Table 1 Results of XRD patterns of TiO₂ gels

Sample	Temperature/ °C	R_{101} / nm	Crystallinity/ %	a /nm	c /nm
Zn-TiO ₂	100	3.8	57.01	0.3810	0.9479
	300	4.8	57.92	0.3796	0.9475
	500	5.7	59.37	0.3791	0.9488
TiO ₂	100	5.6	51.18	0.3798	0.9499
	300	8.5	60.45	0.3789	0.9503
	500	11.2	60.93	0.3790	0.9507

There is no diffraction peak of phase containing Zn in Zn-TiO₂ films, 1% Zn is too low to be detected, but according to the Scherrer equation [18], the grain size of Zn-TiO₂ films is relatively small and the degree of crystallinity gets slightly lower than pure-TiO₂ (Table 1).

To analyze the changes of presence status Zn²⁺ in preparation of Zn-TiO₂ sol, the hydroxyl and chloride ions are considered to be important factors. OH⁻ and Cl⁻ ions often exist in solution simultaneously, while Zn²⁺, apart from forming chlorine with Cl⁻ ions, can also form Zn(OH)₂ and ZnOH⁺ hydroxyl complexes; Zn hydroxides, during the heating process, will become ZnO, dispersed on TiO₂ surface; while Zn²⁺ and Ti⁴⁺ ionic radii are 0.074 nm and 0.068 nm, respectively, the misfit of the two ionic radii is 8.82%, Zn²⁺ can be located in gap position of lattice or replace the position of Ti⁴⁺ in TiO₂ lattice [19].

3.2 FTIR analysis

The FTIR spectra of the Zn-TiO₂ gels after heat treatment are shown in Fig. 2. The broad peaks lying at 400–900 cm⁻¹ (at 888.08 cm⁻¹ for the specimen after 100 °C heat treatment) are characteristic vibration peaks of [TiO₆] ligand, which are attributed to the asymmetric stretching vibration and bending vibration of Ti—O bond; the peaks responding to Zn—O vibration bond appear around 462 cm⁻¹ [20]; the NH₄⁺ absorption peaks are at 1400 cm⁻¹; and the peaks of 1640 cm⁻¹ are H—O—H bending vibration, related to the constitution water; and the peaks at 3000–3400 cm⁻¹ are arisen from stretching vibration of the surface hydroxyl groups of O—H, generally generated by the free water (such as adsorbed water on surface); and the peaks at 3837.77 cm⁻¹ are Ti³⁺—O—H vibration absorption, belonging to —OH vibration area. The spectra show the Zn and TiO₂ combining by a chemical bond, also prove Ti³⁺ existing on Zn-TiO₂ surface. The presence of Ti³⁺ will produce oxygen vacancies in the Zn-TiO₂ and increase the adsorption of O₂ on Zn-TiO₂ surface. Ti³⁺ will react with O₂, generating O₂⁻, then react with the photo-generated holes, thereby reducing the recombination of photo-generated electron-hole pair, thus increasing the Zn-TiO₂ photoelectric response. As the temperature of heat treatment rises, the broad absorption peaks around

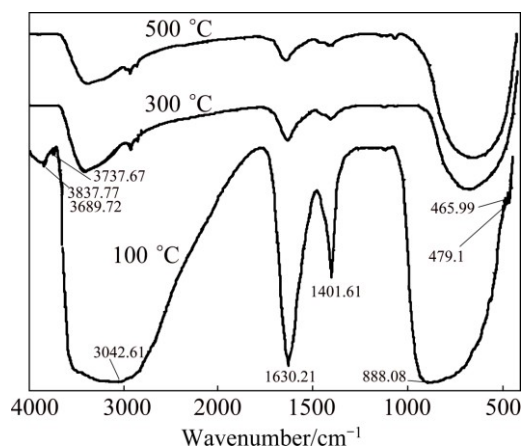


Fig. 2 FTIR curves of Zn-TiO₂ gel

$3000\text{--}3400\text{ cm}^{-1}$ get sharper, which is —OH stretch vibration peak of adsorption water, thus, there are still —OH groups existing on the Zn-TiO_2 surface.

3.3 SEM-EDS analysis

Figure 3 shows the morphology changes of Zn-TiO_2 films after heat treatment. It can be seen that the Zn-TiO_2 films are intact and rough. When the

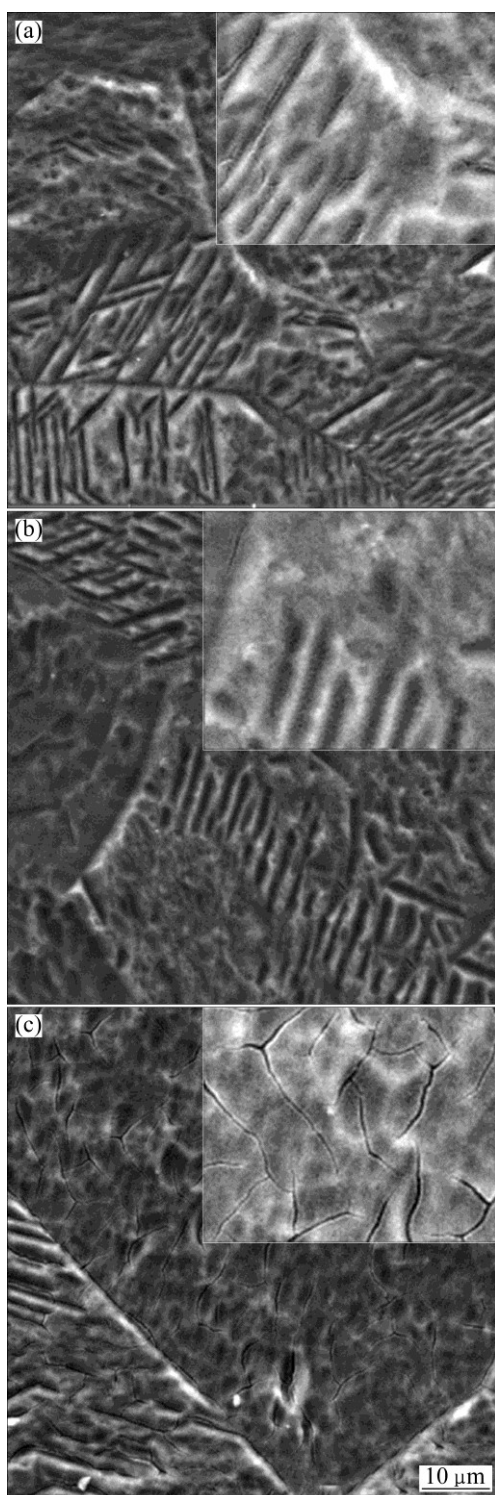


Fig. 3 SEM images of Zn-TiO_2 thin films after heat treatment for 2 h at 100, 300 and 500 °C, respectively

temperature of heat treatment rises to 500 °C, cracks appear on the films, decreasing the corrosion resistance and affecting the photoelectron-chemical performance of Zn-TiO_2 films. The EDS images of elements on Zn-TiO_2 film after heat treatment at 300 °C are shown in Fig. 4. It shows that Zn is unevenly distributed in the TiO_2 film, and that the agglomeration does occur, further indicating that ZnO exists in TiO_2 film in small clusters.

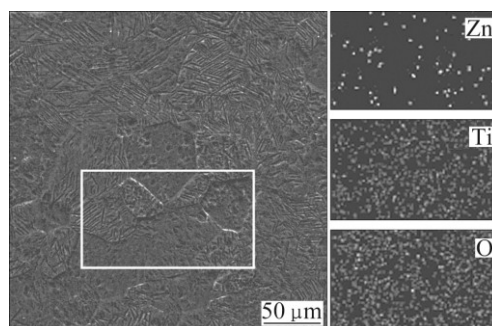


Fig. 4 EDS images of elements on Zn-TiO_2 film surface after heat treatment at 300 °C for 2 h

3.4 UV-vis absorption curve

Figure 5 shows the UV-vis absorption curves of Zn-TiO_2 . It can be seen that Zn-TiO_2 with different heat treatments exhibit an absorption edges around at 400 nm, red-shifted to visible light region, which increases the response of Zn-TiO_2 films to visible light and testifies the improvement of photoelectric performance of Zn-TiO_2 , and Zn-TiO_2 after 300 °C heat treatment displays the maximum extension of visible region. The red-shift of absorption edges implies that the width of band gap gets smaller. This may be caused by the entering of Zn into TiO_2 lattice, which generates impure energy level, thus diminishing the width of band gap. According to the study of YU et al [21], Ti—O—Zn bonding occurs on the surface of TiO_2 during heat treatment, which destroys the original crystal structure of TiO_2 . From our analysis, Zn also exists in small ZnO

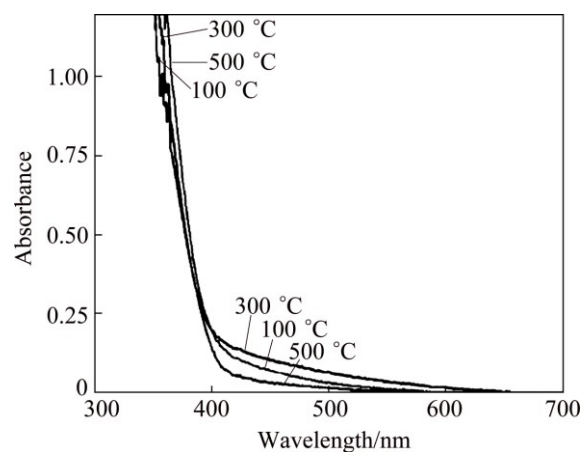


Fig. 5 UV-vis absorption curves of Zn-TiO_2 gels

clusters in TiO_2 , those ZnO clusters interact with crystal structure of TiO_2 , inducing lattice deformation which may induce the red-shift of absorption edges; meanwhile, interband transition occurs between the grains of ZnO and TiO_2 , as shown in Fig. 6.

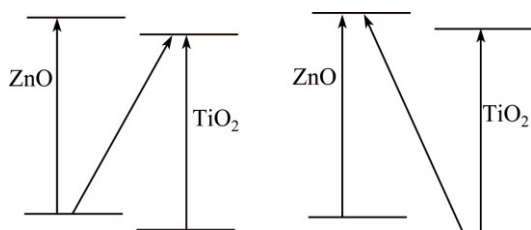


Fig. 6 Transition between energy bands of ZnO– TiO_2

3.5 Open circuit potential (OCP) analysis

The OCP–time curves of Zn– TiO_2 and pure- TiO_2 films after different heat treatments under illumination and dark conditions are shown in Fig. 7. Under the illumination, photo-generated electrons are produced, which can effectively migrate, leading to the decline of the open circuit potential of matrix. From Fig. 7, the potential of electrode significantly drops immediately at 200 s with the illumination. The amplitude of negative shift represented by V_{oc} implies the photoelectrochemical

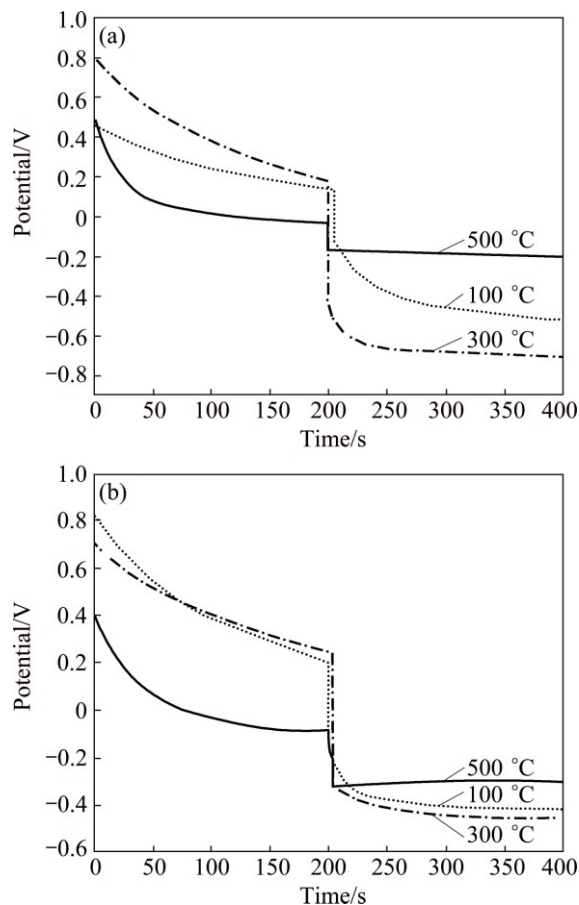


Fig. 7 Time dependence of open-circuit potential of Zn– TiO_2 (a) and pure- TiO_2 (b) treated at different temperatures for 2 h

response and cathodic protection capability of films. After 100, 300 and 500 °C heat treatment, the V_{oc} of Zn– TiO_2 is 649, 897, 174 mV, respectively, which are much larger than those of 493, 544, 238 mV of pure- TiO_2 . Moreover, the lowest potential of Zn– TiO_2 is –710 mV after 300 °C heat treatment, 260 mV lower than pure- TiO_2 (–450 mV), proving that Zn-doping effectively improves the photoelectrochemical anticorrosion performance of TiO_2 , and Zn– TiO_2 film after 300 °C heat treatment shows the best photocathodic protection.

XRD results indicate the effects of Zn^{2+} doping on crystal structure of TiO_2 , which further affect their photoelectrochemical performance. On one hand, the decreased crystallinity and the defects of crystal become the capture center of photogenerated-electron hole, which hampers the separation of photogenerated-electron hole; meanwhile, the smaller grains and higher specific surface area increase the diffusion rate of photogenerated-electron holes into the surface, and facilitate the separation of photogenerated-electron hole, increase the yield of quantum and enhance the photoelectrochemical response. Effects of heat treatment temperature on the optical performance work in a similar way: as the temperature increases, the degree of crystallinity improves, which facilitates the separation of photogenerated-electron hole; meanwhile, with the increase of temperature, accompanied by larger grain and smaller specific surface area, the diffusion path of the hole to the surface increases, the photogenerated electrons-hole pair recombination rate increases, which is unfavorable for photoelectrochemical response. Otherwise, the sample after 500 °C heat treatment shows the smallest V_{oc} , probably due to the appearance of microcracks on TiO_2 film surface, which decreases the photoelectrochemical response of this film.

3.6 Mott–Schottky analysis

To further characterize the photoelectronic properties of the TiO_2 , the Mott–Schottky (M–S) measurements were carried out at the optimum frequency of 1000 Hz [22], as shown in Fig. 8. Carrier densities and flatband potentials were estimated by using the following equation (for the n -type semiconductor) [23,24]:

$$\frac{1}{C^2} = \frac{2}{\varepsilon\varepsilon_0eN_d} \left(E - E_{fb} - \frac{KT}{e} \right) \quad (1)$$

where C is the capacitance of the space charge layer; ε_0 is the permittivity of the free space (8.85×10^{-12} F/m); ε is the semiconductor dielectric constant (~ 80 for TiO_2 [25]); e is the elementary charge (1.602×10^{-19} C); N_d is the charge carrier density; E is the applied potential; E_{fb} is the flatband potential; K is the Boltzmann's constant (1.38×10^{-23} J/K); T is the temperature of operation; KT/e is so small (~ 25 mV) that it can be ignored.

From Eq. (1), N_d can be determined by the slope of the linear portion of M–S curves, the value of flat band potential E_{fb} is approximately obtained by the intercept of the tangent on the potential axis of M–S curves. The amount of band bending in the space charge layer $E_B = E - E_{fb}$, by parameters N_d and E_{fb} , the semiconductor space-charge layer width W can be calculated by $W = \sqrt{2\epsilon\epsilon_0 E_B / (eN_d)}$.

The plotting of $1/C^2$ vs E of Zn–TiO₂ films is shown in Fig. 8. The slopes of the linear portion of M–S curves are positive, indicating that Zn–TiO₂ films are *n*-type semiconductors. The calculation results are shown in Table 2.

The flat-band potential is an important parameter of semiconductor solution system [26]. The position of Fermi level can be considered approximately the position of the boundary of the conduction band for *n*-type semiconductor [27]. Relationship between flat-band potential and Fermi level is $E_{fb} = -eE_F$ (E_F is Fermi level), if flat-band potential negatively shifts and Fermi level rises, which means the reducing power of excited electrons on conduction band gets stronger, and electrons can be more easily transferred to H⁺ to generate H₂, ultimately improving the photoelectric effect [28]. From the results of M–S curves of Table 2, the flat-band potentials of Zn–TiO₂ and TiO₂ all decrease with the

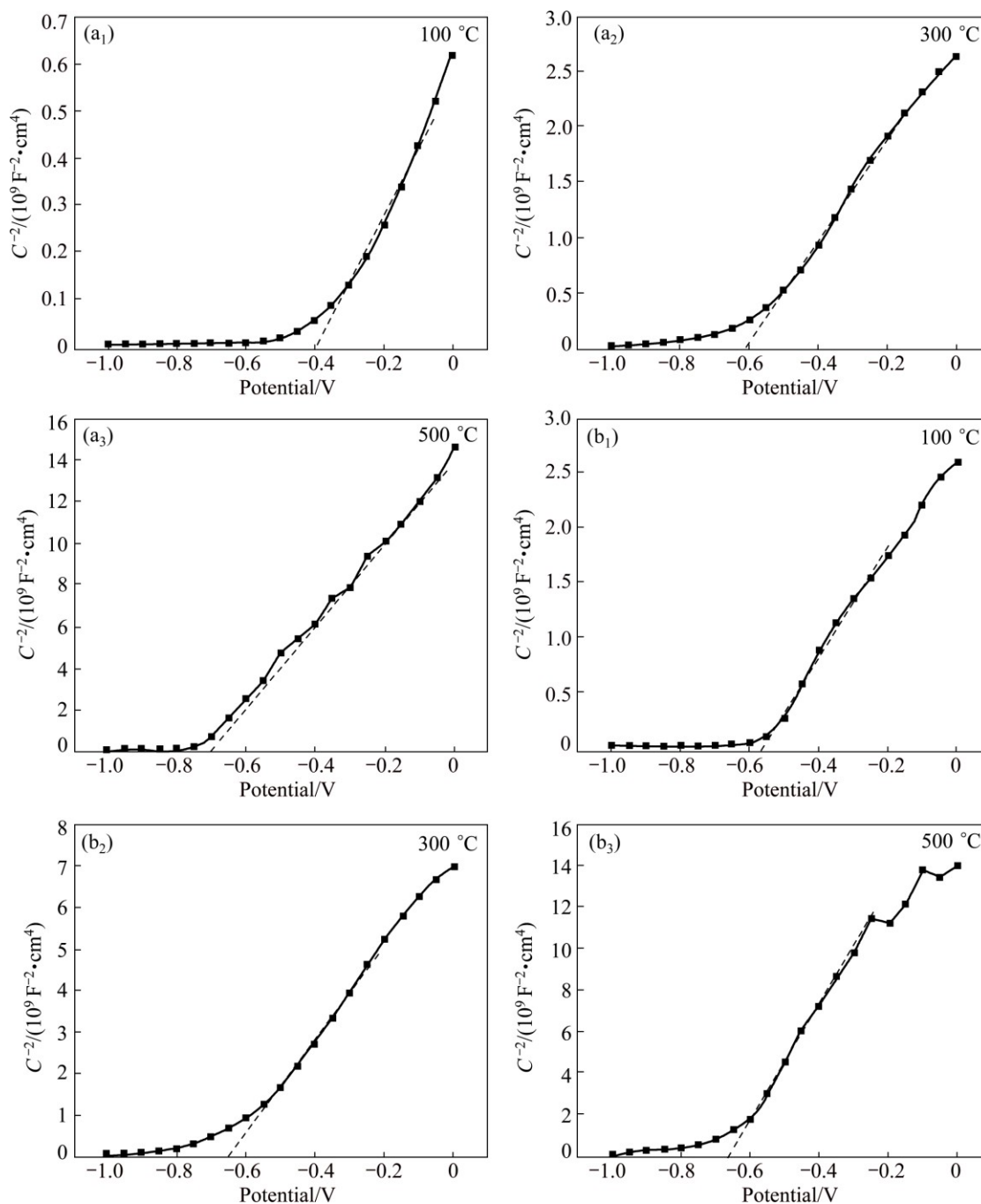


Fig. 8 $1/C^2$ vs E plots of Zn–TiO₂ films (a) and pure-TiO₂ films (b)

Table 2 Parameters of band structure of TiO₂ films treated at different temperatures

Sample	Temperature/°C	N_d/cm^{-3}	E_{fb}/V	W/nm
Zn–TiO ₂	100	1.069×10^{21}	-0.39	9.098
Zn–TiO ₂	300	4.325×10^{20}	-0.63	25.59
Zn–TiO ₂	500	9.357×10^{19}	-0.70	61.50
TiO ₂	100	3.456×10^{20}	-0.56	20.24
TiO ₂	300	1.541×10^{20}	-0.64	37.03
TiO ₂	500	6.428×10^{19}	-0.66	60.97

increase of heat-treatment temperature, while the difference of the flat-band potentials between samples after 300 °C and 500 °C heat treatment is small. Moreover, the Zn–TiO₂ films, except the specimens treated at 100 °C, show lower flat-band potential and stronger reducing capacity of photo-generated electrons than pure-TiO₂.

It can be seen from Table 2 that as the heat-treatment temperature increases, the carrier density N_d shows a decreasing trend in this order: 100, 300, 500 °C. Conversely, the width of space-charge layer shows an increasing trend from 100 to 500 °C.

Carrier density N_d is intrinsic semiconductor performance parameters. The higher the N_d is, the higher the conductivity of the semiconductor becomes; this, however, reduces the width of the space-charge layer W and narrows the electron and hole effective separation zone, which is not favorable for the transfer of photogenerated electron. With N_d being lower, even though the W has been increased, the carrier concentration within the semiconductor has been reduced in the meantime; this increases impedance of the semiconductor itself, which is not favorable for the electronics to participate in the photoelectric response. Therefore, only when the optimum values of W and N_d exist in the photoelectric reaction can the photoelectric performance be effectively improved.

In this experiment, the Zn–TiO₂ film treated at 300 °C shows the best photoelectrochemical performance. The reason probably is that the flat-band potential of this film is low, reducing ability of the photo-generated electrons is strong, and also the synergistic effect of the width of the space-charge layer and carrier density.

4 Conclusions

1) Zn-doped TiO₂ films have been successfully prepared on titanium substrates by a sol–gel method, which exhibit a highly efficient photocathodic protection performance than pure-TiO₂ films, and the open circuit potential of Zn–TiO₂ after 300 °C heat treatment

significantly dropped by 897 mV to -710 mV under an illumination.

2) Compared with the pure-TiO₂ film, the doping of Zn leads to finer grain size and small ZnO clusters existing in Zn–TiO₂ films; ultraviolet visible absorption spectra prove that the light absorption of the Zn–TiO₂ shifts to the visible region.

3) Mott–Shottky curves show that as the heat-treatment temperature of TiO₂ increases, the flat-band potential decreases, carrier density reduces, while the width of the space-charge layer increases. Moreover, for Zn–TiO₂ films, the flat-band potential is lower and carrier density is larger than that of pure-TiO₂, which suggests that under the synergy of W , N_d and flat-band potential, Zn–TiO₂ after 300 °C heat-treatment presents the best photoelectric performance.

References

- [1] CHEN C, YE M D, LV M Q, GONG C, GUO W X, LIN C J. Ultralong rutile TiO₂ nanorod arrays with large surface area for CdS/CdSe quantum dot-sensitized solar cells [J]. *Electrochimica Acta*, 2014, 121: 175–182.
- [2] HE Zhi-qiao, CAI Qiao-lan, FANG Hui-ying, SITU Gao-hua, QIU Jian-ping, SONG Shuang, CHEN Jian-meng. Photocatalytic activity of TiO₂ containing anatase nanoparticles and rutile nanoflower structure consisting of nanorods [J]. *Journal of Environmental Sciences*, 2013, 25(12): 2460–2468.
- [3] LUO Qiang, CAI Qi-zhou, LI Xin-wei, PAN Zhen-hua, LI Yu-jie, CHEN Xi-di, YAN Qing-song. Preparation and characterization of ZrO₂/TiO₂ composite photocatalytic film by micro-arc oxidation [J]. *Transactions of Nonferrous Metals Society of China*, 2013, 23(10): 2945–2950.
- [4] NOVAKOVIC J, VASSILIOU P. Vacuum thermal treated electroless NiP–TiO₂ composite coatings [J]. *Electrochimica Acta*, 2009, 54(9): 2499–2503.
- [5] SHAN C X, HOU X H, CHOY K L. Corrosion resistance of TiO₂ films grown on stainless steel by atomic layer deposition [J]. *Surface and Coatings Technology*, 2008, 202(11): 2399–2402.
- [6] HUA J H, ZHANG C L, CUI B H, BAI K F, GUAN S K, WANG L G, ZHU S J. In vitro degradation of AZ31 magnesium alloy coated with nano TiO₂ film by sol–gel method [J]. *Applied Surface Science*, 2011, 257(21): 8772–8777.
- [7] LI S N, WANG Q, CHEN T, ZHOU Z H, WANG Y, FU J J. Study on cerium-doped nano-TiO₂ coatings for corrosion protection of 316 L stainless steel [J]. *Nanoscale Research Letters*, 2012, 7(15): 227–235.
- [8] LEI C X, ZHOU H, WANG C, FENG Z D. Self-assembly of ordered mesoporous TiO₂ thin films as photoanodes for cathodic protection of stainless steel [J]. *Electrochimica Acta*, 2013, 87(1): 245–249.
- [9] LI J, LIN C J, LI J T, LIN Z Q. A photoelectrochemical study of CdS modified TiO₂ nanotube arrays as photoanodes [J]. *Thin Solid Films*, 2011, 519(16): 5494–5502.
- [10] LIU Y, XU C, FENG Z D. Characteristics and anticorrosion performance of Fe-doped TiO₂ films by liquid phase deposition method [J]. *Applied Surface Science*, 2014, 314: 392–399.
- [11] YUAN J, TSUJIKAWA S. Characterization of sol–gel-derived TiO₂ coatings and their photoeffects on copper substrates [J]. *Journal of the Electrochemical Society*, 1995, 142 (10): 3444–3450.
- [12] ZHANG J, DU R G, LIN Z Q, ZHU Y F, GUO Y, QI H Q, XU L,

- LIN C J. Highly efficient CdSe/CdS co-sensitized TiO₂ nanotube films for photocathodic protection of stainless steel [J]. *Electrochimica Acta*, 2012, 83(12): 59–64.
- [13] SUN M M, CHEN Z Y, YU J Q. Highly efficient visible light induced photoelectrochemical anticorrosion for 304 SS by Ni-doped TiO₂ [J]. *Electrochimica Acta*, 2013, 109: 13–19.
- [14] LI J, LIN C J, LAI Y K, DU R G. Photogenerated cathodic protection of flower-like, nanostructured, N-doped TiO₂ film on stainless steel [J]. *Surface and Coatings Technology*, 2010, 205(2): 557–564.
- [15] ZHANG Y, WANG L L, LIU B K, ZHAI J L, FAN H M, WANG D J, LIN Y H, XIE T F. Synthesis of Zn-doped TiO₂ microspheres with enhanced photovoltaic performance and application for dye-sensitized solar cells [J]. *Electrochimica Acta*, 2011, 56(18): 6517–6523.
- [16] LI F, GUAN L, DAI M, FENG J, YAO M. Effects of V and Zn codoping on the microstructures and photocatalytic activities of nanocrystalline TiO₂ films [J]. *Ceramics International*, 2013, 39(7): 7395–7400.
- [17] WANG K P, TENG H S. Zinc-doping in TiO₂ films to enhance electron transport in dye-sensitized solar cells under low-intensity illumination [J]. *Physical Chemistry Chemical Physics*, 2009, 11(41): 9489–9496.
- [18] ZHANG Q, GAO L, GUO J. Effects of calcination on the photocatalytic properties of nanosized TiO₂ powders prepared by TiCl₄ hydrolysis [J]. *Applied Catalysis B: Environmental*, 2000, 26(3): 207–215.
- [19] ZHAO Y, LI C, LIU X, GU F, DU H L, SHI L. Zn-doped TiO₂ nanoparticles with high photocatalytic activity synthesized by hydrogen-oxygen diffusion flame [J]. *Applied Catalysis B: Environmental*, 2008, 79(3): 208–215.
- [20] ZHENG Y, CHEN C, ZHAN Y, LIN X, ZHENG Q, WEI K, ZHU J, ZHU Y. Luminescence and photocatalytic activity of ZnO nanocrystals: Correlation between structure and property [J]. *Inorganic Chemistry*, 2007, 46(16): 6675–6682.
- [21] YU Xi-bin, YANG Liang-zhun, YANG Shi-ping, ZHOU Chun-lei, XU Xiao-lin, TANG Jing-fen, PENG Xiu-dong. Synthesis and luminescence of SrZnO₂:Eu³⁺, Li⁺ phosphor by long wavelength UV excitation [J]. *Journal of the Chinese Rare Earth Society*, 2005, 23(5): 533–536. (in Chinese)
- [22] MORISON S R. *Electrochemistry at semiconductor and oxidized metal electrodes* [M]. New York: Plenum Press, 1981.
- [23] BÜCHLER M, SCHMUKI P, BÖHNI H. A light reflectance technique for thickness measurements of passive films [J]. *Electrochimica Acta*, 1997, 43(5): 635–637.
- [24] JOHN S E, MOHAPATRA S K, MISRA M. Double-wall anodic titania nanotube arrays for water photooxidation [J]. *Langmuir*, 2009, 25(14): 8240–7.
- [25] LENG Wen-hua, ZHANG Zhao, CHENG Shao-an, ZHANG Jian-qing, CAO Chu-nan. A study of Titanium oxide film electrodes prepared by direct thermal oxidation. preparation, structure and electrochemical properties [J]. *Chinese Journal of Chemical Physics*, 2001, 14(6): 705–710. (in Chinese)
- [26] SANG L X, ZHANG Z Y, BAI G M, DU C X, MA C F. A photoelectrochemical investigation of the hydrogen evolving doped TiO₂ nanotube arrays electrode [J]. *International Journal of Hydrogen Energy*, 2012, 37(1): 854–859.
- [27] HWANG D W, KIM J, PARK T J, LEE J S. Mg-doped WO₃ as a novel photocatalyst for visible light-induced water splitting [J]. *Catalysis Letters*, 2002, 80(1–2): 53–57.
- [28] WANG Bao-hui, WANG De-jun, LI Tie-jin. Studies on photoelectrochemical properties of porous silicon [J]. *Chemical Journal of Chinese University*, 1997, 18(4): 621–624. (in Chinese)

溶胶凝胶法制备 Zn 掺杂 TiO₂ 薄膜的表征和光电化学行为

乔丽英^{1,2}, 谢奉好³, 谢明辉¹, 龚才华¹, 王维朗¹, 高家诚¹

1. 重庆大学 材料科学与工程学院, 重庆 400045;

2. 重庆大学 国家镁合金材料工程技术研究中心, 重庆 400044;

3. 四川师范大学 化学与材料科学学院, 成都 610068

摘要: 采用溶胶-凝胶法在纯钛基体上制备 Zn 掺杂纳米 TiO₂ 薄膜(Zn-TiO₂), 研究不同热处理温度下 Zn 掺杂对纳米 TiO₂ 薄膜的物理性能、光阴极保护效果和光电化学性能的影响。研究表明, 与未掺杂 TiO₂ 薄膜相比, Zn 的加入提高了 Zn-TiO₂ 薄膜的光电化学响应, 在 300 °C 热处理后的薄膜使金属基体的电极电位下降最大, 降低了 897 mV。SEM-EDS 分析表明, Zn 在掺杂薄膜中的分布不均匀, XRD 结果显示 Zn 掺杂的薄膜比未掺杂的薄膜晶粒更细小。红外光谱结果表明, TiO₂ 晶粒表面有 Zn—O 键生成。紫外光谱表明, Zn 掺杂使 Zn-TiO₂ 吸收带边红移, 扩大了 TiO₂ 的光响应范围。根据 Mott-Shottky 曲线可知, Zn-TiO₂ 薄膜比纯 TiO₂ 薄膜的平带电位更负, 载流子量更大。这说明在平带电位、载流子量和空间电荷层宽度的协同作用下, 300 °C 热处理后的 Zn-TiO₂ 薄膜表现了最佳的光电化学响应。

关键词: TiO₂ 薄膜; 锌掺杂; 光阴极保护; 光电化学性能; 溶胶凝胶法

(Edited by Xiang-qun LI)